Hindawi
Shock and Vibration
Volume 2018, Article ID 7859510, 14 pages
https://doi.org/10.1155/2018/7859510

Research Article

Pitch Controller Design of Wind Turbine Based on Nonlinear PI/PD Control

Feihang Zhou and Jun Liu

College of Automation, Xi'an University of Technology, No. 5 Jinhua South Road, Xi'an, China

Correspondence should be addressed to Jun Liu; 1309681265@qq.com

Received 17 May 2018; Revised 23 August 2018; Accepted 3 September 2018; Published 11 October 2018

Academic Editor: Mario Terzo

This paper analyzed and discussed the nonlinear PI/PD control for wind energy conversion system (WECS) pitch controller design. The nonlinear PI/PD controller consists of a classical PI/PD controller and a nonlinear gain table. In this paper, the detailed design procedures of the controller including not only the selection of control parameters but also the formulation of nonlinear gain table were given. In order to verify the effectiveness and correctness of the algorithm, a detailed 2 MW simulation test platform based on MATLAB/SIMULINK environment was established. Meanwhile, some valuable conclusions were also obtained. The presented contents of this article have the reference value and guiding significance for practical engineering application.

1. Introduction

With the global climate problem increasingly prominent and nonrenewable energy sources being largely consumed, the exploration and utilization of renewable energy sources such as wind energy and solar energy have been paid to a high attention. As the fastest growing renewable energy sources in the recent years [1–4], wind generation is the most prevalent in coastal regions spanning temperate and boreal climates. Countries such as China, USA, Denmark, and Canada possess significant wind power potential due to their high average wind velocities [5–8]. Hence, the research and development about wind power have much practical value nowadays. Compared with the constant speed-constant frequency power system, the greatest advantage of variable speed-constant frequency wind power system widely used is the ability to get access to the maximum energy conversion. Mainstream variable speed-constant frequency power generation models include doubly-fed induction generator (DFIG) and permanent magnet synchronous generator (PMSG). Compared with DFIG, PMSG has many superior characteristics such as more efficient performance, higher reliability, and wider speed control range and is gradually becoming the first choice [9]. Therefore, the WECS based on PMSG was selected for research in this paper.

As Figure 1 shows, according to the wind speed, the working region of WECS typically can be divided into two regions, namely, partial-load region that has wind speed below the rated wind speed and full-load region that has wind speed above the rated wind speed. In the partial-load region, the control goal of the wind power system is generally to capture the maximum wind energy in order to achieve the maximum economic benefit. At this time, the partial-load region can also be called the maximum power point tracking (MPPT) region. In the full-load region, the variable propeller is particularly important. At this time, the generator-output power is limited at the rated value by the pitch control since the capacity of the generator and converter is limited [10, 11]. Furthermore, pitch control is also needed in some special working conditions such as the limited power control under rated wind speed, the low-voltage crossing in power grid, power grid needs to be injected into the inertia, and lighten the wind turbine loads. Meanwhile, it is pointed out that pitch control can also smoothen the power [12]. This paper focuses on the pitch control above the rated wind speed.

Figure 2 illustrates the pitch-controlled system. Obviously, Figure 2(a) depicts the blades action under pitch-controlled, and Figure 2(b) shows the variable-pitch drive system in wind turbine hub. The variable-pitch drive system consists of pitch drive cabinet, variable-pitch drive,

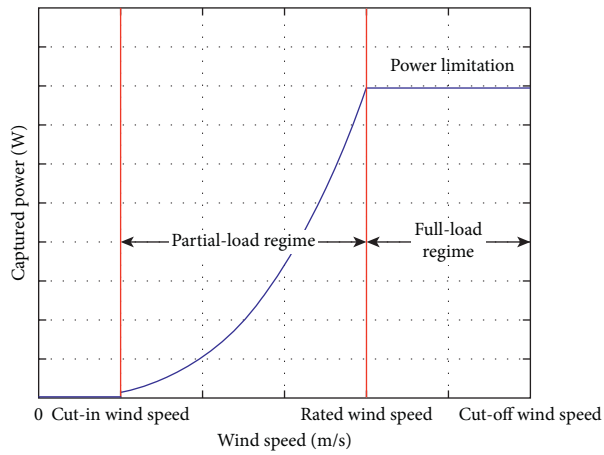

Figure 1: WECS operation modes in different wind speeds.

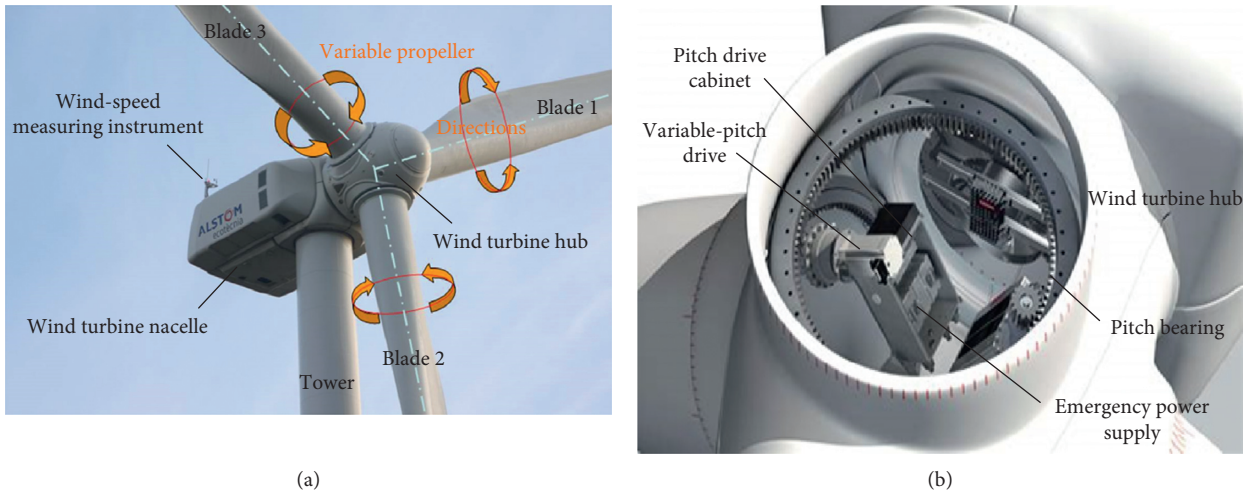

(a) (b)

Figure 2: Pitch-controlled system. (a) Blades action under pitch-controlled. (b) Variable-pitch drive system in wind turbine hub.

emergency power supply, pitch bearing and variable-pitch lubrication systems. The pitch control system and communication system are in the pitch drive cabinet. In general, the pitch controller and master controller are connected by the optical fiber communication. The PROFIBUS or CANopen protocols are generally used in this communication. Usually, the master controller sends the pitch instructions to the pitch controller and gets some important information from it at the same time. When the instructions are obtained, the pitch controller starts to control the variable-pitch drive-operating system.

At present, the research on variable-pitch control mainly includes two main categories: linear control and nonlinear control. The research of the linear controller mainly has PI/PD control, $H\infty$ controller with a linear matrix inequality approach [13], linear quadratic Gaussian LQR control [14], and generalized predictive control (GPC) [15]. The nonlinear control mainly contains LPV control [16] and some intelligent control methods such as fuzzy control [17]. Because wind turbine is a multi-input multi-output system containing strongly nonlinear dynamics, the effect of nonlinear control is better than the linear control. Taking into account the complexity of the algorithm, the most applied controllers in engineering is still PI/PD control. Therefore, the design of the variable propeller with the nonlinear PI/PD controller considering the nonlinear characteristics of the wind turbine has become the key. So, this article takes this as the focus of the study and summarizes some valuable conclusions. And this study can also provide the necessary reference and guidance for the follow-up engineering practice.

The structure of this paper is as follows: the dynamic model and structure of WECS is briefly introduced in Section 2. Section 3 explains the controller design in details, including the controller parameter tuning and the calculation of nonlinear gain. In Section 4, the validation of the nonlinear PI/PD controller is surveyed using the MATLAB/Simulink simulator. Finally, Section 5 provides some useful conclusions.

2. Mathematical Model of WECS

WECS is mainly constitutive of wind turbine, transmission chain, permanent magnet synchronous generator, generator-side converter, DC bus, and the grid-side inverter. Its structure is shown in Figure 3.

2.1. Wind Turbine Model. Based on the Baez theory, the aerodynamic power, P_t and torque T_t of the wind turbine are [18–22]

$$\begin{cases} P_t = 0.5\pi\rho R^2 C_P(\beta,\lambda)v^3, \\ T_t = \dfrac{P_t}{\omega_t} = \dfrac{0.5\pi\rho R^3 C_P(\beta,\lambda)v^2}{\lambda}, \end{cases} \tag{1}$$

where ρ is the air density, R is the radius of wind wheel, v is the wind speed, β is the pitch angle, ω_t is the speed of wind turbine, λ is the tip speed ratio (TSR), and C_P is defined as the wind energy conversion coefficient. A 2 MW baseline wind turbine-power coefficient is shown in Figure 4. Obviously, C_P is the function of β and λ.

The tip-speed ratio λ is given by

$$\lambda = \frac{R\omega_t}{v}. \tag{2}$$

2.2. Dynamic Model of PMSG. If PMSG was supposed to be an ideal motor, it should meet the following criteria:

(1) three-phase stators are symmetry.

(2) induced electromotive force is sinusoidal.

(3) there is no damping winding on the rotor

(4) magnetic saturation of iron core, vortex, and hysteresis loss can be neglected.

(5) electronic conductivity of permanent magnet material is zero.

Under this assumption, the mathematical model of PMSG [23, 24] is

$$\begin{pmatrix} L_d & 0 \\ 0 & L_q \end{pmatrix}\begin{pmatrix} \dot{i}_d \\ \dot{i}_q \end{pmatrix} = \begin{pmatrix} -R_s & n_p\omega_g L_q \\ -n_p\omega_g L_d & -R_s \end{pmatrix}\begin{pmatrix} i_d \\ i_q \end{pmatrix} + \begin{pmatrix} u_d \\ u_q \end{pmatrix} + \begin{pmatrix} 0 \\ n_p\omega_g\Psi \end{pmatrix}. \tag{3}$$

Electromagnetic torque is given by

$$T_g = 1.5n_p\left[\left(L_d - L_q\right)i_d i_q + \Psi i_q\right], \tag{4}$$

where L_d and L_q are the d-axis and q-axis stator reluctance, R_s is the stator resistance, Ψ is the permanent flux, n_p is pole pairs, ω_g is the speed of PMSG, i_d and i_q are d-axis and q-axis currents, respectively, and u_d and u_q are d-axis and q-axis voltages, respectively.

Because nonsalient PMSG meets $L_d = L_q = L$, the mathematical model of PMSG has coupling terms such as $n_p\omega_{gen}i_q$, $-n_p\omega_{gen}(i_d + \Psi/L)$, according to Equation (3).

Given

$$\begin{pmatrix} v_d \\ v_q \end{pmatrix} = \begin{pmatrix} 0 & n_p\omega_g L \\ -n_p\omega_g L & 0 \end{pmatrix}\begin{pmatrix} i_d \\ i_q \end{pmatrix} + \begin{pmatrix} 0 \\ -n_p\omega_g\Psi \end{pmatrix} + \begin{pmatrix} u_d \\ u_q \end{pmatrix}. \tag{5}$$

The mathematical model of PMSG could be rewritten as

$$\begin{pmatrix} \dot{i}_d \\ \dot{i}_q \end{pmatrix} = \begin{pmatrix} \dfrac{-R_s}{L} & 0 \\ 0 & \dfrac{-R_s}{L} \end{pmatrix}\begin{pmatrix} i_d \\ i_q \end{pmatrix} + \begin{pmatrix} \dfrac{1}{L} & 0 \\ 0 & \dfrac{1}{L} \end{pmatrix}\begin{pmatrix} v_d \\ v_q \end{pmatrix}. \tag{6}$$

The above formula also can be rewritten into a transfer function $G_0(s)$.

$$G_0(s) = \frac{i_d(s)}{v_d(s)} = \frac{i_q(s)}{v_q(s)} = \frac{1}{Ls + R_s}. \tag{7}$$

Figure 5 shows the inner control of current. The closed loop transfer function of the current or torque can be obtained by Figure 5. And the closed loop transfer function also could be taken as a first-order inertial system.

$$\begin{aligned} \varphi(s) &= \frac{i_d}{i_{dref}} = \frac{i_q}{i_{qref}} = \frac{T_g}{T_{g\_ref}} \\ &= \frac{k_{iP}s + k_{iI}}{Ls^2 + (R_s + k_{iP})s + k_{iI}} = \frac{1}{\tau_T s + 1}, \end{aligned} \tag{8}$$

$$\tau_T = \frac{R_s}{k_{iI}} = \frac{L}{k_{iP}}, \tag{9}$$

where τ_T is the inertial time constant and T_{g_ref} is the command signal of T_g.

Equation (8) shows that the dynamic model of PMSG could be equivalent to a first-order inertial system by current feedforward decoupling control and first-order tuning for PI parameters. Usually, when $\tau_T \le 0.01$, we can leave out the inertial time delay of PMSG.

2.3. Dynamics of Blade Pitch Actuator. There are two kinds of drives in the blade pitch actuator at present. They are the motor drive and hydraulic drive. Compared with the hydraulic drive, motor drive has the characteristics of lower cost and higher reliability and has been widely used. Actual motor drive is shown in Figure 6.

The collecting variable-pitch strategy was used. According to Figure 7, the blade dynamics is expressed as

$$J_{Blade}\ddot{\beta} = T_{Drive} - (\mu + f)\dot{\beta}. \tag{10}$$

By leaving out the inertia time delay of the motor drive, the drive torque of motor is assumed as

$$T_{Drive} = \left(K_{\beta D}s + K_{\beta P}\right)\left(\beta_{ref} - \beta\right). \tag{11}$$

The blade pitch actuator dynamic can be given by Figure 8 where β_{ref} is the command of β and the PD parameters of the blade pitch actuator are $K_{\beta P}$ and $K_{\beta D}$.

If the delay coefficient meets

$$\tau_\beta = \frac{\mu + f}{K_{\beta P}} = \frac{J_{Blade}}{K_{\beta D}}, \tag{12}$$

the blade pitch actuator dynamic model can be simplified as

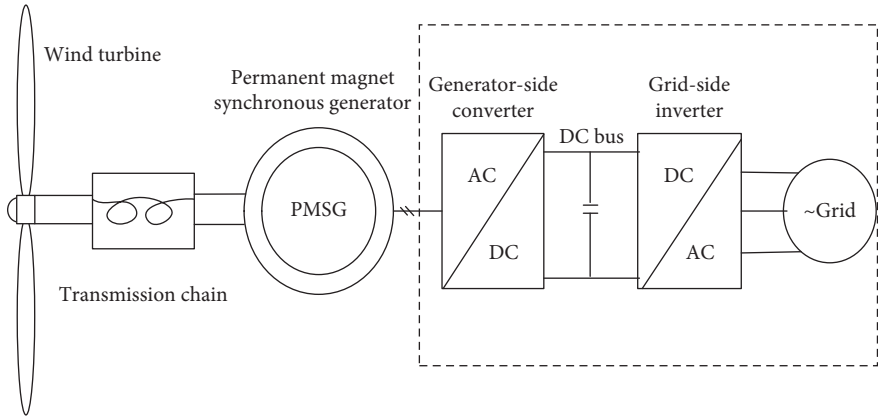

Figure 3: Structure diagram of WECS.

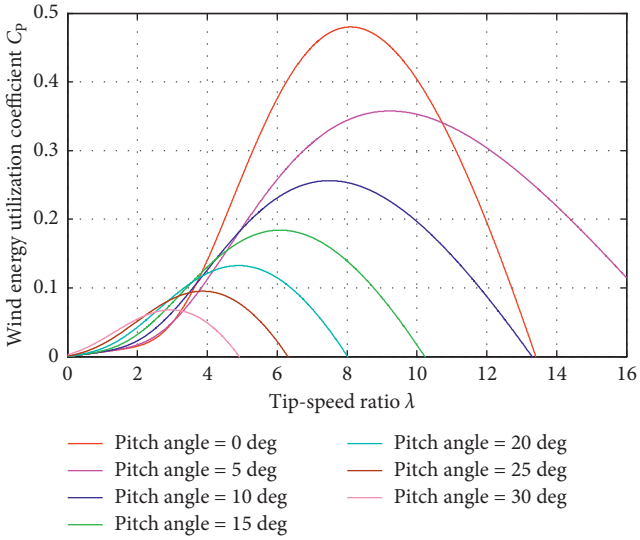

Figure 4: 2-MW baseline wind turbine power coefficient.

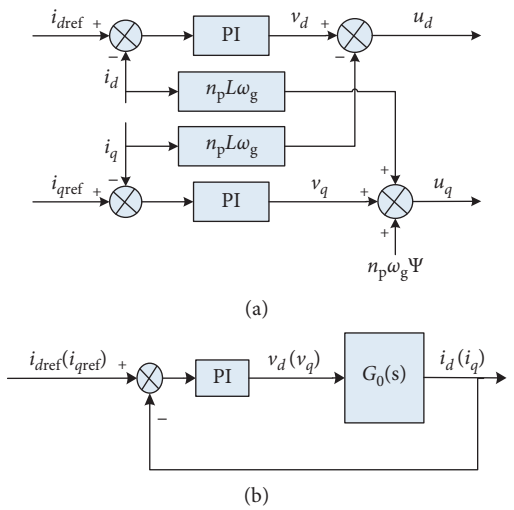

Figure 5: Inner control of current (remark: PI parameters are denoted as k_{iP} and k_{iI}). (a) Current feedforward decoupling control. (b) First-order tuning for PI parameters.

$$G_\beta(s) = \frac{\beta(s)}{\beta_{\text{ref}}(s)} = \frac{1}{\tau_\beta s + 1}. \tag{13}$$

Obviously, the inertia delay coefficient, τ_β in Equations (12) and (13) can be reduced by increasing PD parameters. When $K_{\beta P}$ and $K_{\beta D}$ take the appropriate value, the inertia delay can also be left out. Actually, because the value of the parameters J_{Blade}, μ, and f is unknown, the value of the control parameters $K_{\beta P}$ and $K_{\beta D}$ can only depend on experience.

2.4. Dynamic Model of Transmission Chain. Figure 9 shows the generator cabin internal components of high-speed permanent magnet wind turbine. It is clear that its transmission chain mainly consists of spindle (or low-speed shaft), gearbox, and high-speed shaft. The dynamics of the transmission chain is characterized by Figure 10.

According to Figure 10, the dynamics of the transmission chain is derived as

$$\begin{cases} J_t\dot{\omega}_t = T_t - D_t\omega_t - T_{\text{Sun}}, \\ J_g\dot{\omega}_g = T_{\text{Sate}} - D_g\omega_g - T_g. \end{cases} \tag{14}$$

The gearbox ratio is defined as

$$n = \frac{\omega_g}{\omega_t} = \frac{T_{\text{Sun}}}{T_{\text{Sate}}}. \tag{15}$$

From Equations (14) and (15), the dynamic model of the transmission chain can be simplified as

$$J_{\text{eq}}\dot{\omega}_t = T_t - D_{\text{eq}}\omega_t - nT_g, \tag{16}$$

where

$$\begin{cases} J_{\text{eq}} = J_t + n^2J_g, \\ D_{\text{eq}} = D_t + n^2D_g. \end{cases} \tag{17}$$

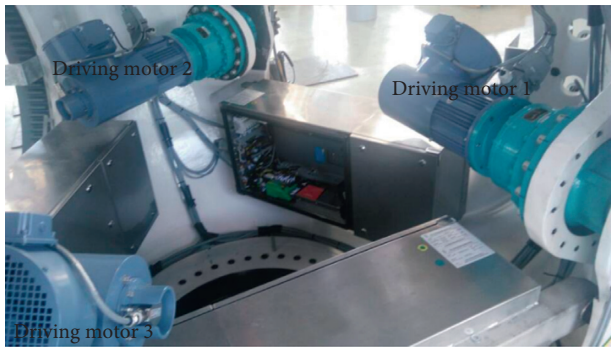

Figure 6: Motor drive system in pitch actuator.

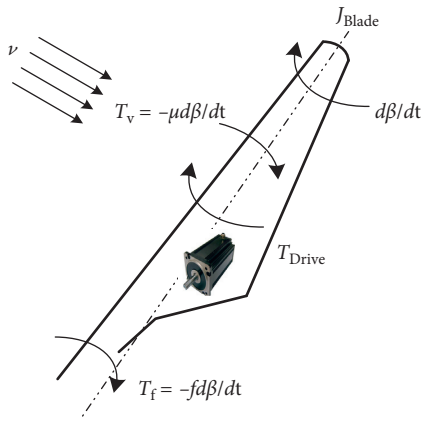

Figure 7: Blade (1, 2, 3) model (note: J_{Blade} is the moment of blade inertia. T_{Drive} is the motor-driving torque. T_v is the resistance torque of wind. T_f is the resistance torque of blade root friction. f and μ are the coefficient of friction of blade root and wind drag, respectively).

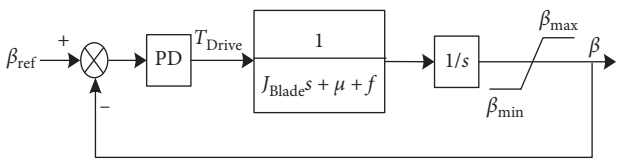

Figure 8: Blade pitch actuator dynamic.

3. Design of Controller

When the wind speed v is above the rated wind v_{rate}, the system needs pitch control to unload the power and enable the speed ω_t to approach the rated speed ω_{rate}. If the inertia delay τ_T and τ_β are neglected by adjusting control parameters, the electromagnetic torque T_g and pitch angle β can be approximated as their command values T_{g_ref} and β_{ref}.

$$\begin{cases} T_g \approx T_{g\_ref} = \dfrac{P_{rate}}{\omega_g} = \dfrac{P_{rate}}{n\omega_t}, \\ \beta \approx \beta_{ref} = \left(k_D s + k_P + \dfrac{k_I}{s}\right)(\omega_t - \omega_{rate}), \end{cases} \tag{18}$$

where s is the Laplace factor.

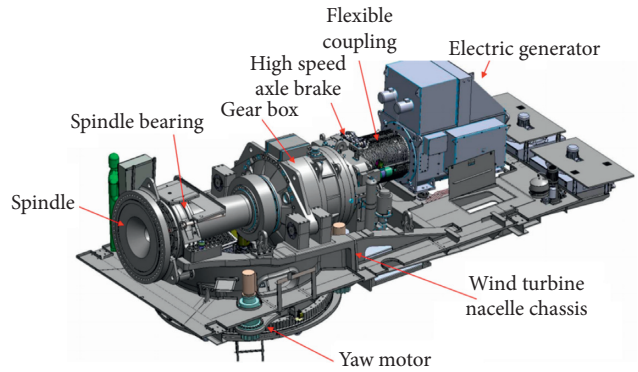

Figure 9: Internal components of generator cabin.

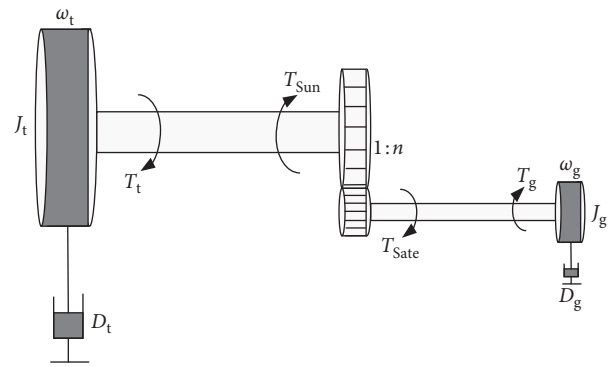

Figure 10: Dynamic model of transmission chain (remark: Sun and Sate represent the sun wheel and planetary gear of gearbox).

By linearizing Equations (1) and (18), the small signal values are

$$\begin{cases} \tilde{T}_t = a\tilde{\beta} + b\tilde{\omega}_t + c\tilde{v} + o\left(\tilde{\beta}, \tilde{\omega}_t, \tilde{v}\right), \\ \tilde{T}_g \approx -\dfrac{P_{rate}}{\overline{\omega}_g^2}\tilde{\omega}_g = -\dfrac{P_{rate}}{n\overline{\omega}_t^2}\tilde{\omega}_t, \\ \tilde{\beta} \approx \left(k_D s + k_P + \dfrac{k_I}{s}\right)\tilde{\omega}_t, \end{cases} \tag{19}$$

where

$$\begin{cases} a = \left.\dfrac{\partial T_t}{\partial \beta}\right|_{op} = \dfrac{\rho\pi R^2 \overline{v}^3}{2\overline{\omega}_t} \cdot \left.\dfrac{\partial C_P}{\partial \beta}\right|_{op}, \\ b = \left.\dfrac{\partial T_t}{\partial \omega_t}\right|_{op} = \dfrac{\rho\pi R^3 \overline{v}^2}{2\overline{\omega}_t}\left(\left.\dfrac{\partial C_P}{\partial \lambda}\right|_{op} - \dfrac{\overline{C}_P}{\overline{\lambda}}\right), \\ c = \left.\dfrac{\partial T_t}{\partial v}\right|_{op} = \dfrac{\rho\pi R^3 \overline{v}}{2}\left(\dfrac{3\overline{C}_P}{\overline{\lambda}} - \left.\dfrac{\partial C_P}{\partial \lambda}\right|_{op}\right), \end{cases} \tag{20}$$

Superscripts ~ and — refer to the small signal value and mean value, respectively. o is high-order infinitesimal.

Meanwhile, Equation (16) can also be rewritten as

$$J_{eq}\left(\dot{\overline{\omega}}_t + \dot{\tilde{\omega}}_t\right) = \overline{T}_t + \tilde{T}_t - D_{eq}\left(\overline{\omega}_t + \tilde{\omega}_t\right) - n\left(\overline{T}_g + \tilde{T}_g\right). \quad (21)$$

By eliminating the mean value of the upper equation and Equations (19) and (22) can be obtained.

$$\left[\frac{\left(J_{eq} - ak_D\right)s^2 + \left(D_{eq} - ak_P - b - \left(P_{rate}/\overline{\omega}_t^2\right)\right)s - ak_I}{s}\right]\tilde{\omega}_t = c\tilde{v}. \quad (22)$$

Due to $a < 0$, k_D can increase the inertia of the system. In general, k_D and k_I are not used at the same time because they have the opposite effect on the system, namely, either PI control or PD control can be used in pitch control.

3.1. Design of Nonlinear PI Controller. When $k_D = 0$, Equation (22) could be rewritten as

$$\begin{cases} d(s)\tilde{\omega}_t = \dfrac{c}{J_{eq}}s\tilde{v}, \\ d(s) = s^2 + \dfrac{D_{eq} - b - \left(P_{rate}/\overline{\omega}_t^2\right) - ak_P}{J_{eq}}s + \dfrac{-ak_I}{J_{eq}}. \end{cases} \quad (23)$$

By comparing $d(s)$ with the typical second-order system, we get

$$d(s) = s^2 + 2\zeta\omega_n + \omega_n^2. \quad (24)$$

Equation (22) can be obtained.

$$\begin{cases} \omega_n = \sqrt{\dfrac{-ak_I}{J_{eq}}}, \\ \zeta = \dfrac{D_{eq} - b - \left(P_{rate}/\overline{\omega}_t^2\right) - ak_P}{2\sqrt{-ak_I J_{eq}}}. \end{cases} \quad (25)$$

Figure 11 shows the torque characteristics of WECS. Obviously, there are two equilibrium points A and B in the system. For equilibrium point B, if there is a perturbation increasing the rotor speed, then PMSG torque will be over wind turbine torque. After the perturbation is eliminated, rotor speed can decrease. By the same method, we can also confirm the system will be back to point B by the assumption that a little perturbation reduced the rotor speed. Hence, the working point B is stable. It could be confirmed that the equilibrium point A is unstable by this perturbation observation method. Therefore, only the point B is a stable equilibrium point, and the range of stability is $\omega_t \geq \omega_A$. The slope of wind turbine torque characteristic, T_t is b and the slope of PMSG torque characteristic, nT_g is $-P_{rate}/\overline{\omega}_t^2$. When the system works at the point B, we can get Equation (26) by Figure 11.

$$0 > -\frac{P_{rate}}{\overline{\omega}_t^2} > b. \quad (26)$$

Generally, the damping D_{eq} is unknown. From Equation (26), the damping ratio ζ in Equation (25) meets

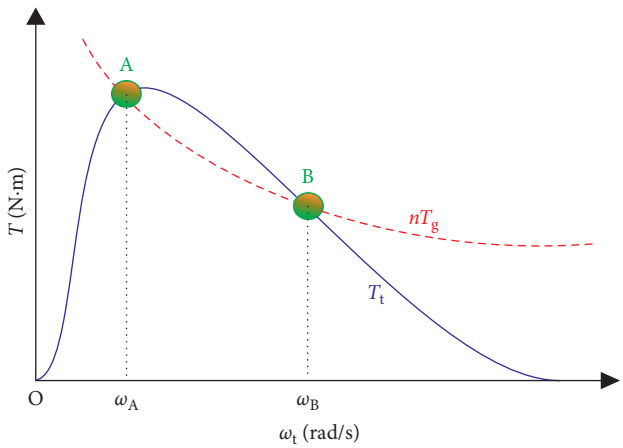

Figure 11: Torque characteristics of WECS.

$$\zeta > \frac{-ak_P}{2\sqrt{-ak_I J_{eq}}}. \quad (27)$$

Given $(-ak_P)/(2\sqrt{-ak_I J_{eq}}) = \varepsilon \geq 1$ and

$$\begin{cases} -ak_P = K_P, \\ -ak_I = K_I, \end{cases} \quad (28)$$

the damping ratio ζ and PI parameters will meet $\zeta > \varepsilon$ and $K_P^2 = 4K_I J_{eq}\varepsilon^2$. Therefore, the parameters K_P and K_I are given by

$$\begin{cases} K_P = 2J_{eq}\omega_n\varepsilon, \\ K_I = J_{eq}\omega_n^2. \end{cases} \quad (29)$$

By the assumption of $K_P = \eta_I K_I$, Equation (29) could be rewritten as

$$\begin{cases} \omega_n = \dfrac{2\varepsilon}{\eta_I}, \\ K_P = \dfrac{4J_{eq}\varepsilon^2}{\eta_I}, \\ K_I = \dfrac{4J_{eq}\varepsilon^2}{\eta_I^2}. \end{cases} \quad (30)$$

3.2. Design of Nonlinear PD Controller. Inertia has the ability to prevent frequency mutation in the system. Low frequency oscillation and rotor oscillation of the system can be suppressed by increasing inertia. Therefore, PD control-providing the virtual inertia for the system, is often applied to the small inertia systems and situations that need to be injected into inertia.

Similarly, when $k_I = 0$, Equation (22) also could be rewritten as

$$\left[\left(J_{eq} - ak_D\right)s + \left(D_{eq} - b - \frac{P_{rate}}{\overline{\omega}_t^2} - ak_P\right)\right]\tilde{\omega}_t = c\tilde{v}. \quad (31)$$

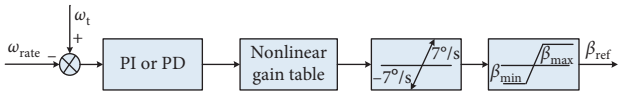

Figure 12: Pitch control based on nonlinear PI or PD controller.

If $D_{eq} - b - P_{rate}/\overline{\omega}_t^2$ in Equation (31) is neglected, the transfer function $G_{v\omega}$ is given by

$$\begin{cases} G_{v\omega}(s) = \dfrac{\tilde{v}(s)}{\tilde{\omega}(s)} \approx \dfrac{c}{-ak_P} G_0(s), \\ G_0(s) = \dfrac{1}{\left(\left(J_{eq} - ak_D\right)/\left(-ak_P\right)\right)s + 1}. \end{cases} \tag{32}$$

Given

$$\begin{cases} -ak_P = K_P, \\ -ak_D = K_D, \end{cases} \tag{33}$$

and $K_D = \eta_D J_{eq}$, the parameter K_P is

$$K_P = \left(J_{eq} + K_D\right)\mathrm{BW} = \left(1 + \eta_D\right)J_{eq}\mathrm{BW}, \tag{34}$$

where BW is the bandwidth of $G_0(s)$.

In general, we keep K_D and K_P (or K_I and K_P) fixed and make $-1/a$ as a nonlinear gain table. Meanwhile, the limit of the variable pitch rate and angle is taken into account, and pitch control based on nonlinear PI or PD controller is shown in Figure 12.

3.3. Nonlinear Gain Table. Obviously, all of the wind speed $\overline{v}$, rotor speed of wind turbine $\overline{\omega}_t$, and pitch angle $\overline{\beta}$ can have effect on the nonlinear gain a by Equation (20). But, the sensitivity of the system to the pitch angle is far greater than other factors generally. When the system works at the rated working point $\overline{\omega}_t = \omega_{rate}$ and $\overline{T}_t = T_{rate}$, the relationship between $\overline{v}$ and $\overline{\beta}$ is

$$\frac{\pi\rho R^2 C_P\left(\overline{\beta}, \left(R\overline{v}\right)/\omega_{rate}\right)\overline{v}^3}{2\omega_{rate}} = T_{rate}. \tag{35}$$

In general, the nonlinear gain a only depends on the pitch angle $\overline{\beta}$. The calculation process of nonlinear gain is shown in Figure 13, and the parameters of WECS are shown in Table 1.

In practice, the function $C_P(\beta, \lambda)$ can only be obtained by data fitting, and these data for fitting are generated by Bladed Software. In order to verify the correctness of the algorithm shown in Figure 8, an empirical formula of C_P is used.

$$\begin{cases} C_P(\beta, \lambda) = 0.5176\left(\dfrac{116}{\lambda_m} - 0.4\beta - 5\right)e^{-(21/\lambda_m)} + 0.0068\lambda, \\ \dfrac{1}{\lambda_m} = \dfrac{1}{\lambda + 0.08\beta} - \dfrac{0.035}{\beta^3 + 1}. \end{cases} \tag{36}$$

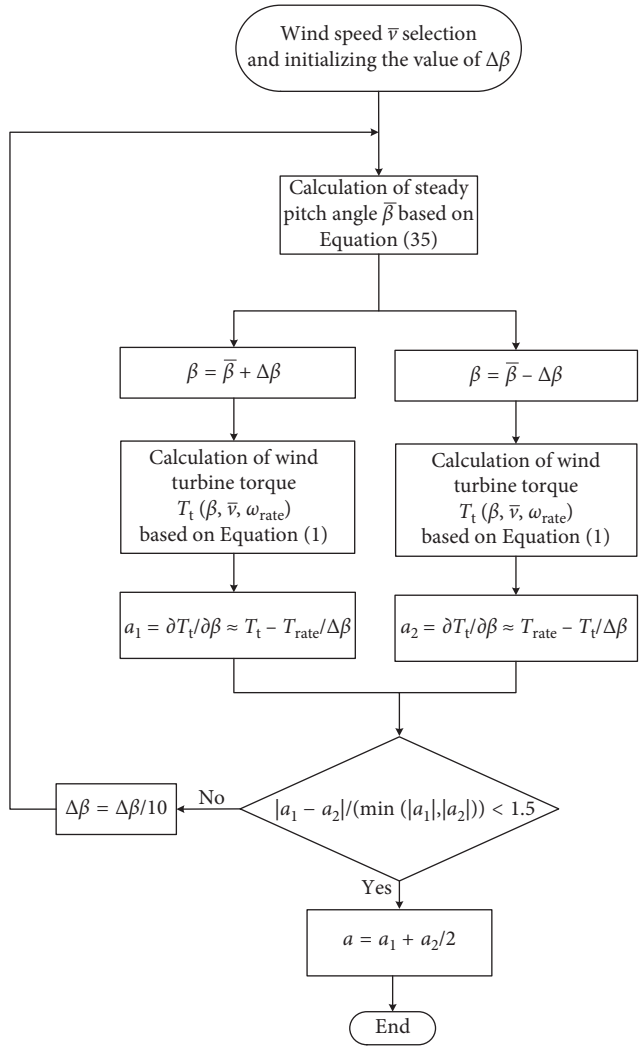

Figure 13: The calculation process of nonlinear gain a (remark: $\Delta\beta$ is the precision value of β, and the initial value of $\Delta\beta$ is 0.01°).

Table 1: WECS parameters.

Parameters	Value
Equivalent moment of inertia J_{eq} (kg·m^2)	2×10^4
Equivalent damping coefficient D_{eq}	100
Blade length R (m)	28
Gear box ratio n	100
Air density ρ (kg/m^3)	1.225
Cut-out wind speed v_{Out} (m/s)	25
Inertia delay coefficient of blade pitch actuator τ_β	0.01
Inertia delay coefficient of torque control τ_T	0.01
Rated power P_{rate} (MW)	2
Rated torque T_{rate} (kN·m)	10^3
Rate rotor speed ω_{rate} (rad/s)	2
Rated wind speed v_{rate} (m/s)	12
Generator pole logarithm	3
Permanent flux (Wb)	1.25
Maximum power coefficient $C_{P\ max}$	0.48

Table 2: Nonlinear gain a.

Wind speed $\overline{v}$ (m/s)	Pitch angle $\overline{\beta}$ (°)	Nonlinear gain a_1	Nonlinear gain a_2	Calculated value of a	Truth value of a
11	0.769	−131258	−185437	−158348	−158348
12	2.21	−50628	−52895	−51761	−51760
12.1	2.53	−25142	−54975	−40058	−40057
12.2	2.94	−25702	−38593	−32147	−32147
12.3	3.43	−24971	−30670	−27821	−27821
12.4	3.98	−35384	−16564	−25974	−25974
12.5	4.55	−28240	−22884	−25562	−25562
13	7.3495	−29605	−29670	−29638	−29638
14	12.0014	−24736	−58744	−41740	−41740
15	15.6949	−44415	−65296	−54856	−54856
16	18.7385	−87893	−50143	−69018	−69018
17	21.309	−94964	−73747	−84355	−84355
18	23.518	−97211	−104702	−100956	−100956
19	25.44	−91846	−145894	−118870	−118870
20	27.136	−90789	−185643	−138216	−138216
21	28.64	−143466	−174484	−158975	−158975
22	29.9874	−230630	−131854	−181242	−181242
23	31.1999	−148312	−261735	−205023	−205023
24	32.2981	−244074	−216678	−230376	−230376
25	33.298	−357896	−156795	−257346	−257346

The partial derivative of the upper formula is

$$\begin{cases} \dfrac{\partial C_P}{\partial \beta} = 0.5176 e^{-(21/\lambda_m)} \left[116 \dfrac{\partial (1/\lambda_m)}{\partial \beta} - 0.4 - 21 \dfrac{\partial (1/\lambda_m)}{\partial \beta} \left(\dfrac{116}{\lambda_m} - 0.4\beta - 5 \right) \right], \\ \dfrac{\partial (1/\lambda_m)}{\partial \beta} = \dfrac{-0.08}{(\lambda + 0.08\beta)^2} + \dfrac{0.105\beta^2}{\left(\beta^3 + 1\right)^2}. \end{cases} \tag{37}$$

The truth value of a could be calculated by Equations (20) and (37). Table 2 shows the calculated and truth values of nonlinear gain at different wind speed. From Table 2, the calculated value of a is very close to the truth value of a. Therefore, the algorithm shown in Figure 13 is valid. The minimum of β is 2.21° above the rated wind, and the relationship between $-1/a$ and β is shown in Figure 14,. Nonlinear gain $-1/a$ is

$$-\frac{1}{a(\beta)} = \begin{cases} 9.37 \times 10^{-6}\beta + 5.79 \times 10^{-7}, & 2.21^\circ \le \beta < 4.2^\circ, \\ 3.50 \times 10^{-8}\beta^2 - 2.54 \times 10^{-6}\beta + 4.99 \times 10^{-5}, & 4.2^\circ \le \beta \le 33.298^\circ. \end{cases} \tag{38}$$

4. Validation of Algorithm by Simulation

In this section, simulations are carried out with MATLAB/Simulink environment. And the block diagram of WECS is shown in Figure 15. In order to verify the correctness and effectiveness of nonlinear PI and PD pitch control, a detailed 2 MW simulation test platform of WECS was constructed. The simulation parameters of the system are shown in Table 1, and the function $C_P(\beta, \lambda)$ is the empirical formula.

The step-change wind shown in Figure 16(a) is used to simulate the actual wind condition. And the response of PI control is shown in Figure 17. Given $\eta_I = \varepsilon = 2 \times 10^3$, the PI parameters K_P and K_I were calculated by Equation (30). Meanwhile, simulation results of PD control under step-change wind shown in Figure 16(b) are illustrated in Figure 18. Given $\eta_D = 0.7$ and BW = 50, the PD parameters K_P and K_D were calculated by Equation (34).

Figures 17(a) and 18(a) show the electromagnetic power curves. It is clear that the output power of WECS is maintained at 2 MW, and the power fluctuation with nonlinear gain control is obviously less than the one with fixed parameters control. The generator rotor speed curves are shown in Figures 17(b) and 18(b). Obviously, the speed steady-state errors of PI control is less than the speed steady-state errors of PD control. Figures 17(c) and 18(c) describe

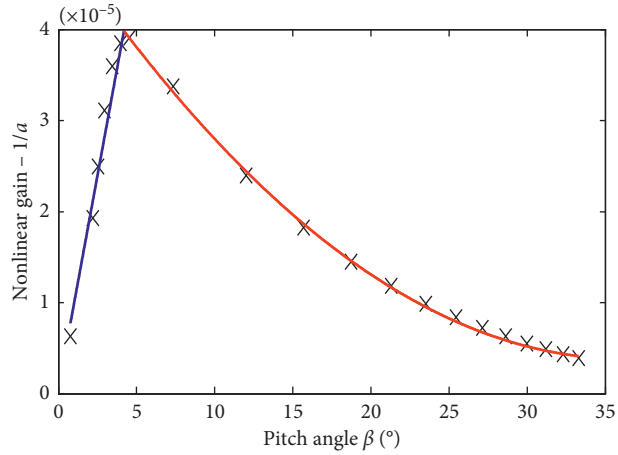

Figure 14: Fitting curve and data.

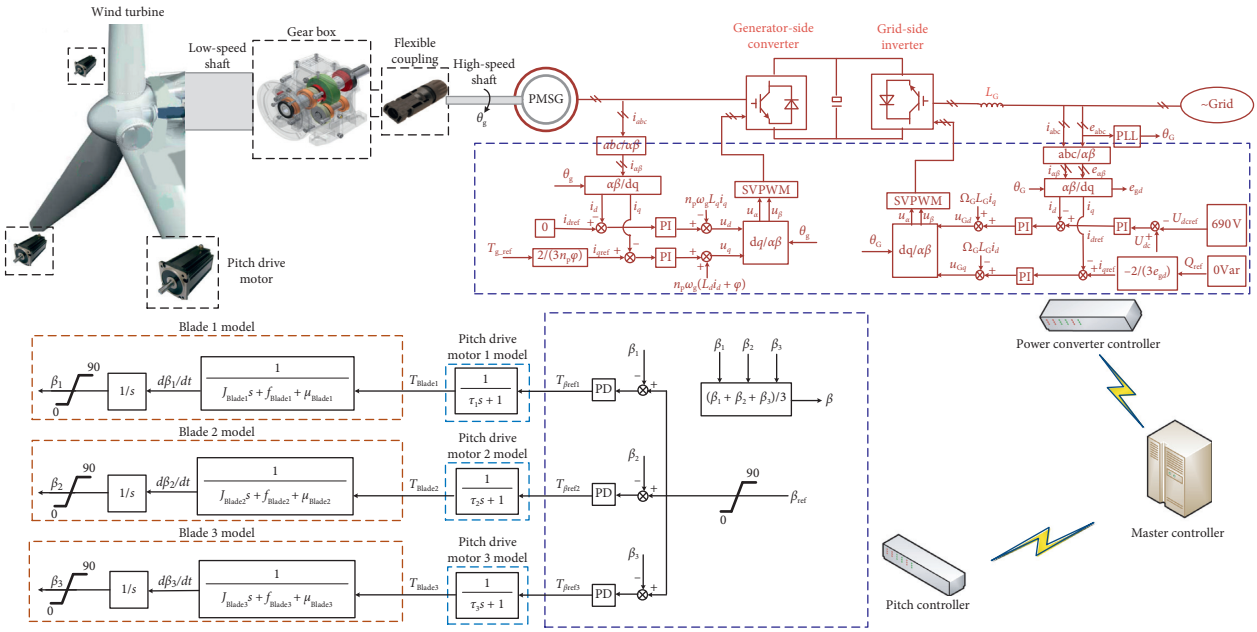

Figure 15: Block diagram of WECS.

the pitch angle curve. Compared with the PI control, the actual value of the pitch angle under PD control failed to achieve the value in Table 2. However, the pitch control is generally used as a coarse control. Therefore, the small pitch angle errors and rotor speed errors of PD control are acceptable. By Figures 17(d) and 18(d), the stator three-phase currents could be observed. The simulation results also indicate that the power of WECS is more sensitive to pitch control than the rotor speed, when the wind speed changes.

In Figure 19(a), the wind speed decays at step change. Under this wind speed, the responses of WECS are shown in Figures 19(b)–19(f). Meanwhile, simulation results under gradual change wind speed shown in Figure 20(a) are given by Figures 20(b)–20(f). Different from other responses curves such as power, torque, and rotor speed, the changes in the pitch angle are not smooth. This is because the rate of pitch angle change is limited at ±7°/s.

By thesis comparisons among classical PI control algorithm, classical PD control algorithm, nonlinear PI control algorithm, and nonlinear PD control algorithm, the similar conclusions could be summed up. Compared with the PD control, PI control has high tracking accuracy and the pitch angle has changed into the right place in Table 2. Under the nonlinear PI/PD control, the output power fluctuate is small. And the output power is very sensitive to the change in pitch angle under different wind conditions. Furthermore, the merits of nonlinear PI/PD control algorithms have been clearly revealed in Figures 19 and 20.

5. Conclusion

In this research, the design procedure of a pitch controller with nonlinear PI/PD control is given in detail, including the selection of PI/PD parameters and the calculation of

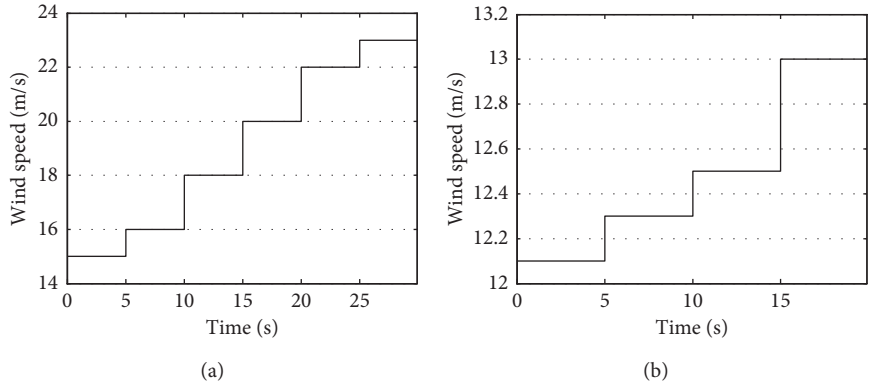

Figure 16: Step-change wind speed.

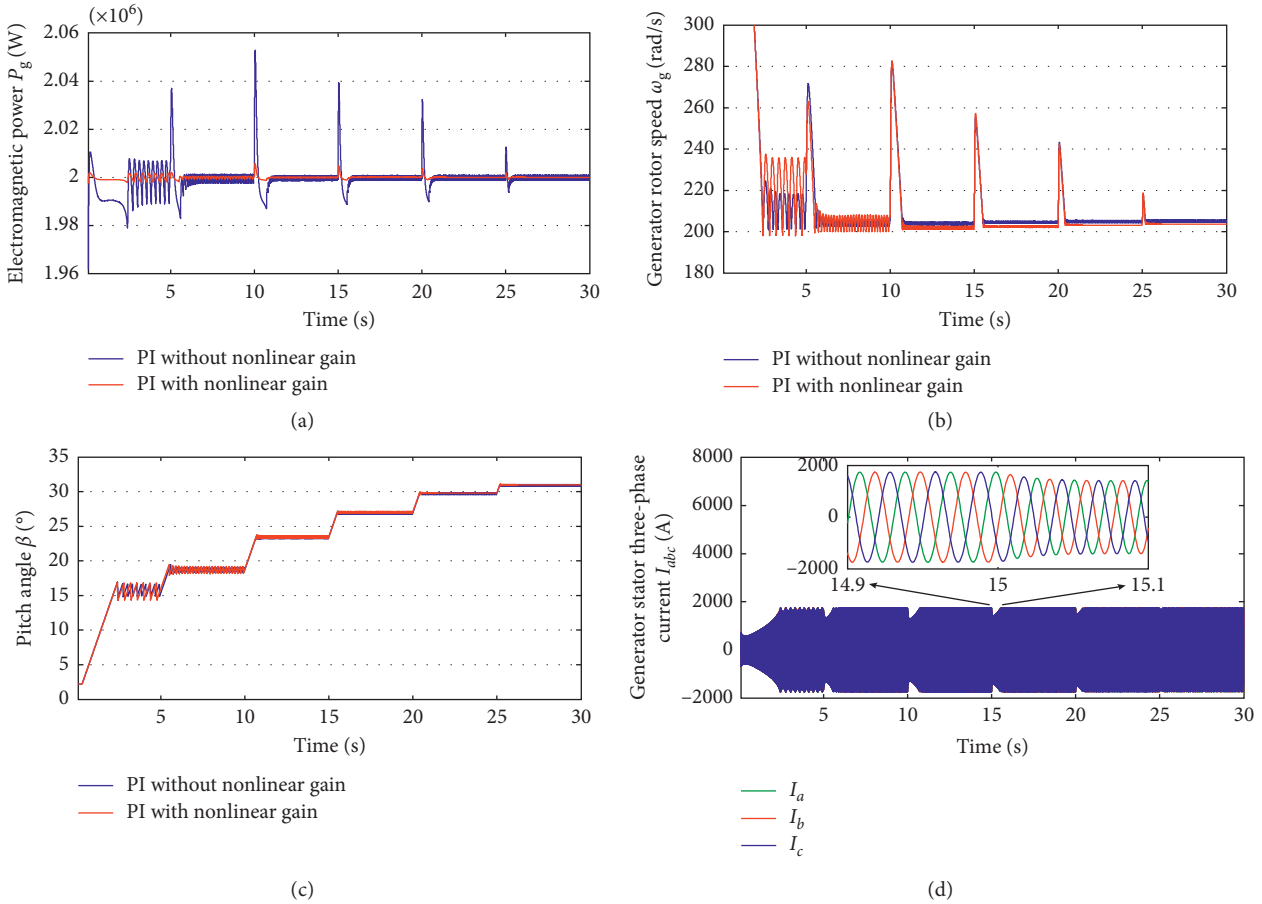

Figure 17: Responses under PI control. (a) Electromagnetic power curve. (b) Generator rotor speed curve. (c) Pitch angle curve. (d) Generator stator three-phase current under PI nonlinear gain.

nonlinear gain. After that, a simulation test platform for a two-megawatt WECS was built. Finally, the effectiveness and correctness of the algorithm was verified by this test platform, and some useful conclusions were summed up:

(i) The output power of WECS is the most sensitive to the change in the pitch angle.

(ii) Compared with the fixed parameters control, the nonlinear control with nonlinear gain can make the power fluctuate smaller.

(iii) The precision of speed tracking is high, and the pitch angle can change into the right place under the PI control, compared with the PD control.

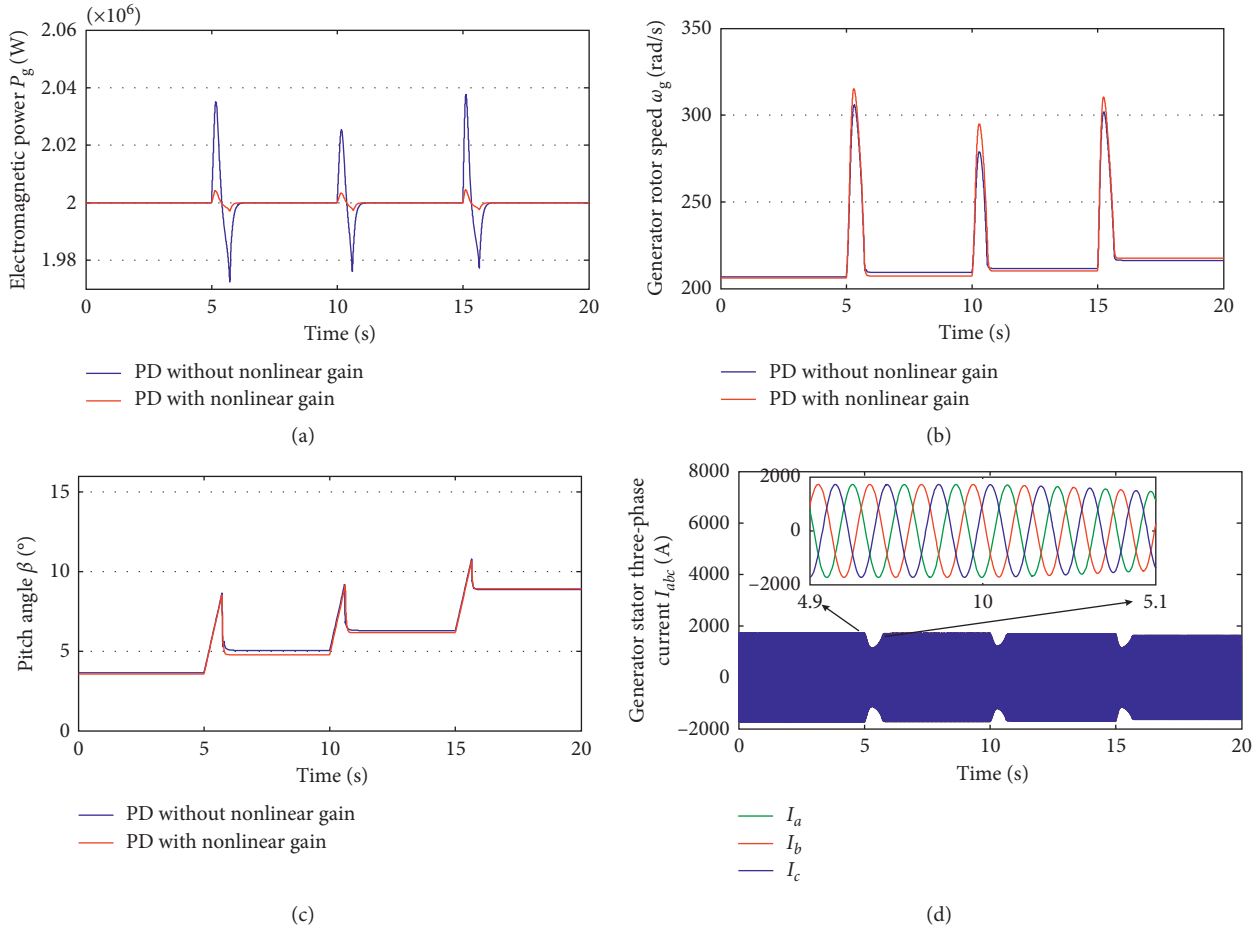

FIGURE 18: Responses under PD control. (a) Electromagnetic power curve. (b) Generator rotor speed curve. (c) Pitch angle curve. (d) Generator stator three-phase current under PI nonlinear gain.

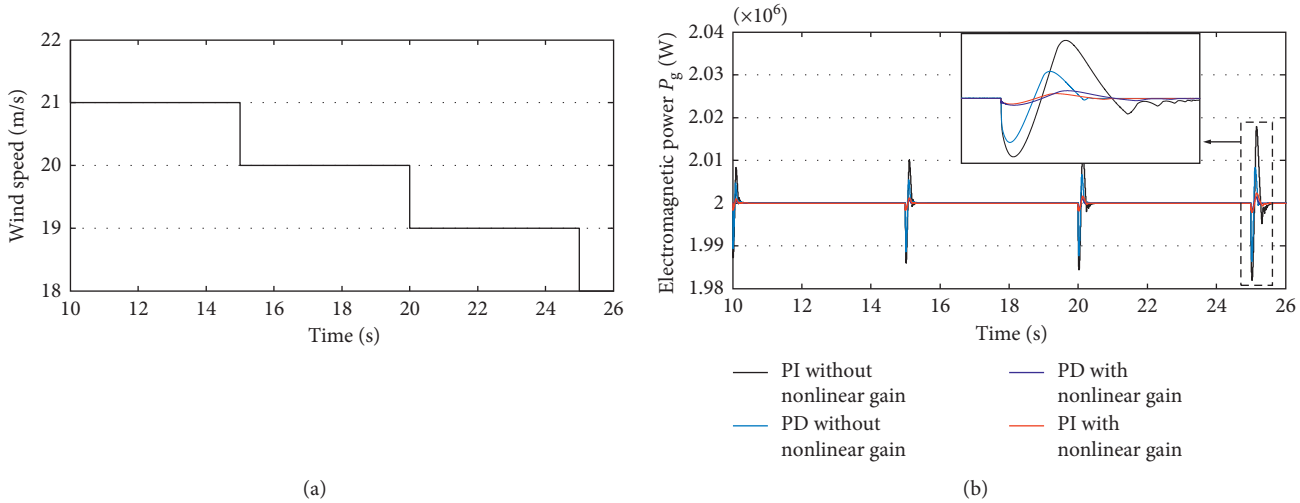

FIGURE 19: Continued.

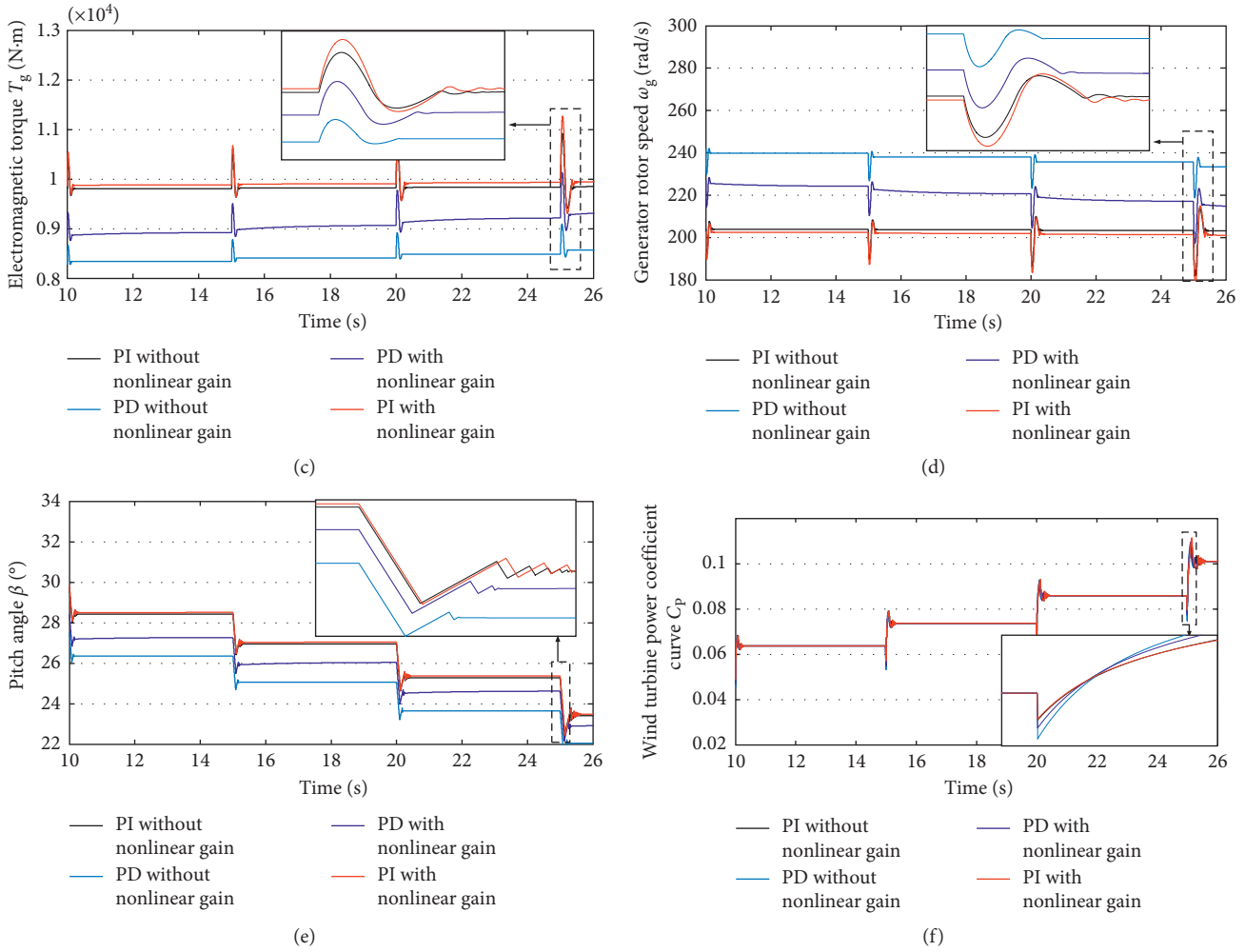

Figure 19: Responses under step-change wind speed. (a) Wind speed curve. (b) Electromagnetic power curve. (c) Electromagnetic torque curve. (d) Generator rotor speed curve. (e) Pitch angle curve. (f) Wind turbine power coefficient curve.

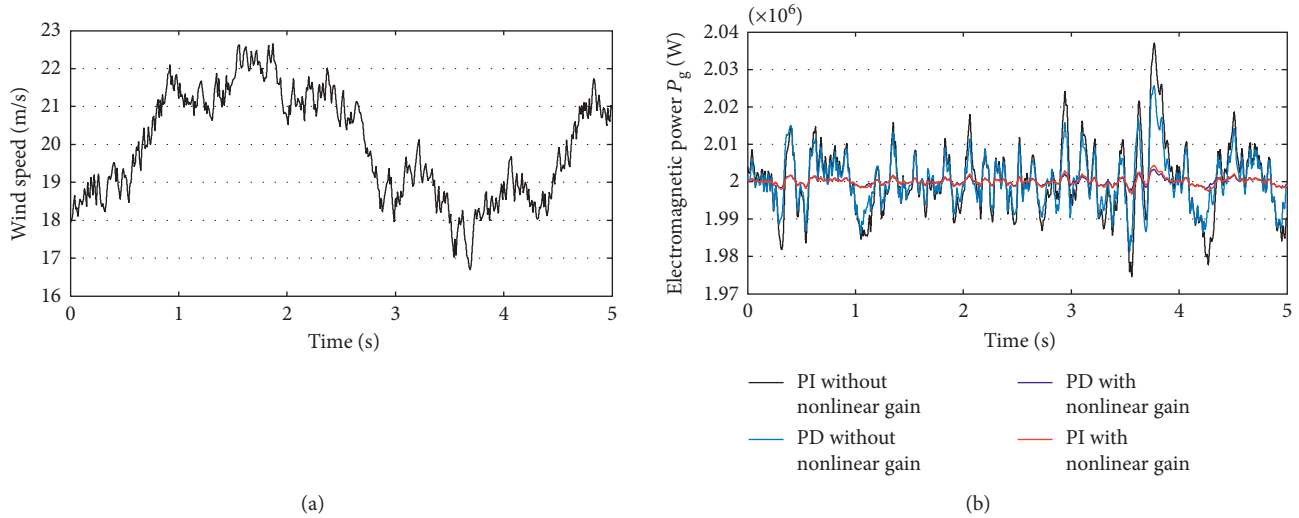

Figure 20: Continued.

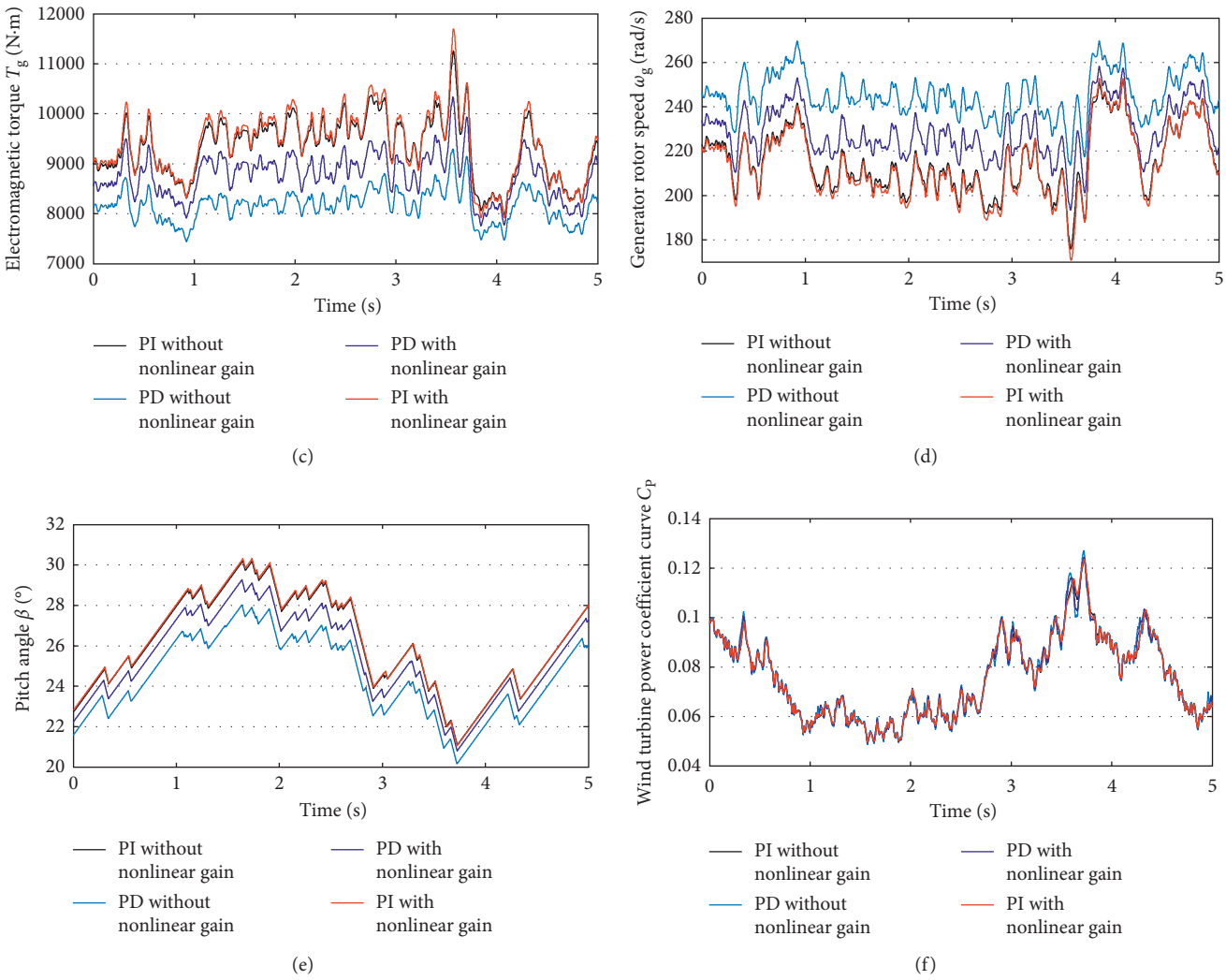

FIGURE 20: Responses under gradual change wind speed. (a) Wind speed curve. (b) Electromagnetic power curve. (c) Electromagnetic torque curve. (d) Generator rotor speed curve. (e) Pitch angle curve. (f) Wind turbine power coefficient curve.

Data Availability

The data used to support the findings of this study are available from the corresponding author upon request.

Conflicts of Interest

The authors declare that there are no conflicts of interest regarding the publication of this paper.

Acknowledgments

The research was supported by Key R&D projects in Shaanxi (Grant no. 2017GY-061).

References

[1] S. Li, T. A. Haskew, R. P. Swatloski, and W. Gathings, "Optimal and direct-current vector control of direct-driven PMSG wind turbines," *IEEE Transactions on Power Electronics*, vol. 27, no. 5, pp. 2325–2337, 2012.

[2] D. X. Llano and R. A. McMahon, "Control techniques with system efficiency comparison for micro-wind turbines," *IEEE Transactions on Sustainable Energy*, vol. 8, no. 4, pp. 1609–1617, 2017.

[3] J. Liu, H. Meng, Y. Hu, Z. Lin, and W. Wang, "A novel MPPT method for enhancing energy conversion efficiency taking power smoothing into account," *Energy Conversion and Management*, vol. 101, pp. 738–748, 2015.

[4] P. Li, R. Dargaville, Y. Cao, D. Y. Li, and J. Xia, "Storage aided system property enhancing and hybrid robust smoothing for large-scale PV systems," *IEEE Transactions on Smart Grid*, vol. 8, no. 6, pp. 2871–2879, 2016.

[5] M. Little and K. Pope, "Performance modelling for wind turbines operating in harsh conditions," *International Journal of Energy Research*, vol. 41, no. 3, pp. 417–428, 2017.

[6] R. Bajric, N. Zuber, G. A. Skrimpas, and N. Mijatovic, "Feature extraction using discrete wavelet transform for gear fault diagnosis of wind turbine gearbox," *Shock and Vibration*, vol. 2016, Article ID 6748469, 10 pages, 2016.

[7] Ł. Doliński, M. Krawczuk, and A. Żak, "Detection of delamination in laminate wind turbine blades using one-dimensional wavelet analysis of modal responses," *Shock*

and Vibration, vol. 2018, Article ID 4507879, 15 pages, 2018.

[8] P. Li, R. X. Li, Y. Cao, D. Y. Li, and G. Xie, "Multi-objective sizing optimization for island microgrids using triangular aggregation model and levy-harmony algorithm," *IEEE Transactions on Industrial Informatics*, vol. 14, no. 8, pp. 3495–3505, 2017.

[9] J. Yan, Y. Feng, H. Lin, Z. Q. Zhu, Y. Huang, and X. Guo, "Improved sliding mode model reference adaptive system speed observer for fuzzy control of direct-drive permanent magnet synchronous generator wind power generation system," *IET Renewable Power Generation*, vol. 7, no. 1, pp. 28–35, 2013.

[10] S. Roy, "Power output by active pitch-regulated wind turbine in presenceof short duration wind variations," *IEEE Transactions on Energy Conversion*, vol. 28, no. 4, pp. 1018–1025, 2013.

[11] N. Horiuchi and T. Kawahito, "Torque and power limitations of variable speed wind turbines using pitch control and generator power control," in *Proceedings of 2001 IEEE Power Engineering Society Summer Meeting*, vol. 1, pp. 638–643, Vancouver, BC, Canada, 2001.

[12] R. M. Kamel, A. Chaouachi, and K. Nagasaka, "Wind power smoothening using fuzzy logic pitch controller and energy capacitor system for improvement micro-grid performance in islanding mode," *Energy*, vol. 35, no. 5, pp. 2119–2129, 2010.

[13] R. Sakamoto, T. Senjyu, T. Kaneko et al., "Output power leveling of wind turbine generator by pitch angle control using H∞ control," in *Proceedings of IEEE PES Power Systems Conference and Exposition*, pp. 2044–2049, Atlanta, GA, USA, October 2006.

[14] U. Shaked and E. Soroka, "On the stability robustness of the continuous time LQG optimal control," *IEEE Transactions on Automatic Control*, vol. 30, no. 10, pp. 1039–1043, 1985.

[15] T. Senjyu, R. Sakamoto, N. Urasaki, T. Funabashi, H. Fujita, and H. Sekine, "Output power leveling of wind turbine generator for all operating regions by pitch angle control," *IEEE Transactions on Energy Conversion*, vol. 21, no. 2, pp. 467–475, 2006.

[16] X. Tong and X. Zhao, "Power generation control of a monopile hydrostatic wind turbine using an H∞ loop-shaping torque controller and an LPV pitch controller," *IEEE Transactions on Control Systems Technology*, vol. 99, pp. 1–8, 2017.

[17] T. L. Van, T. H. Nguyen, and D.-C. Lee, "Advanced pitch angle control based on fuzzy logic for variable-speed wind turbine systems," *IEEE Transactions on Energy Conversion*, vol. 30, no. 2, pp. 578–587, 2015.

[18] B. G. Rawn, P. W. Lehn, and M. Maggiore, "Control methodology to mitigate the grid impact of wind turbines," *IEEE Transactions on Energy Conversion*, vol. 22, no. 2, pp. 431–438, 2007.

[19] M. Toulabi, S. Bahrami, and A. M. Ranjbar, "An input-to-state stability approach to inertial frequency response analysis of doubly-fed induction generator-based wind turbines," *IEEE Transactions on Energy Conversion*, vol. 32, no. 4, pp. 1418–1431, 2017.

[20] D. Y. Li, P. Li, W. C. Cai, Y. D. Song, and H. J. Chen, "Adaptive fault-tolerant control of wind turbines with guaranteed transient performance considering active power control of wind farms," *IEEE Transactions on Industrial Electronics*, vol. 65, no. 4, pp. 3275–3285, 2018.

[21] S. Ebadollahi and S. Saki, "Wind turbine torque oscillation reduction using soft switching multiple model predictive control based on the gap metric and kalman filter estimator," *IEEE Transactions on Industrial Electronics*, vol. 65, no. 5, pp. 3890–3898, 2018.

[22] B. Beltran, T. Ahmed-Ali, and M. El Hachemi Benbouzid, "Sliding mode power control of variable-speed wind energy conversion systems," *IEEE Transactions on Energy Conversion*, vol. 23, no. 2, pp. 551–558, 2008.

[23] L. Trilla, F. D. Bianchi, and O. Gomis-Bellmunt, "Linear parameter-varying control of permanent magnet synchronous generators for wind power systems," *IET Power Electronics*, vol. 7, no. 3, pp. 692–704, 2014.

[24] K. H. Kim, Y. C. Jeung, D. C. Lee, and H. G. Kim, "LVRT scheme of PMSG wind power systems based on feedback linearization," *IEEE Transactions on Power Electronics*, vol. 27, no. 5, pp. 2376–2384, 2012.